

---

# STAMBRIDGE: SPECTRAL-TEMPORAL AMPLITUDE-AWARE MID-FEATURE BRIDGE FOR EEG VISUAL DECODING\*

---

Jiahe Meng<sup>1</sup>, Weiming Zeng<sup>\*1</sup>, Yueyang Li<sup>1,2</sup>, Bo Chai<sup>2</sup>, Hongjie Yan<sup>3</sup>, Zhiguo Zhang<sup>4</sup>, Wai Ting Siok<sup>2</sup>, and Nizhuan Wang<sup>\*2</sup>

<sup>1</sup>Lab of Digital Image and Intelligent Computation, Shanghai Maritime University, Shanghai 201306, China

<sup>2</sup>Department of Language Science and Technology, The Hong Kong Polytechnic University, Hung Hom, Kowloon, Hong Kong SAR, China

<sup>3</sup>Department of Neurology, Affiliated Lianyungang Hospital of Xuzhou Medical University, Lianyungang 222002, China

<sup>4</sup>Institute of Computing and Intelligence, Harbin Institute of Technology Shenzhen, Shenzhen 518000, China

## ABSTRACT

Decoding visual stimuli using electroencephalography (EEG) remains especially challenging due to the significant modality gap between low-SNR neural signals and highly structured vision–language spaces. Unlike auditory signals, which share temporal information with EEG, the high-dimensional spatial nature of visual data makes direct cross-modal alignment inherently more unstable than that of other modalities. To address this, we propose STAMBRIDGE, a versatile two-stage framework that sequentially tackles feature conditioning and cross-modal alignment. First, we introduce a Spectral-Temporal Amplitude-aware Modulation (STAM) to extract well-conditioned EEG representations. By replacing hard frequency masking with amplitude-derived soft channel weighting and multi-scale temporal convolutions, STAM explicitly preserves frequency-aware transients while reducing the risk of time-domain ringing artifacts. Building upon these robust neural features, we further introduce a model-agnostic Mid-Feature Semantic Bridge (MFSB) that constructs a regularized intermediate space through directed cross-modal interactions, enabling staged distillation and more stable semantic alignment. Experiments on the THINGS-EEG benchmark show competitive performance in 200-way zero-shot retrieval, with 34.50% Top-1 and 65.95% Top-5 accuracy. In addition, embeddings learned by STAMBRIDGE produce semantically coherent image reconstructions with a diffusion model, demonstrating robust EEG-to-vision semantic alignment. The code is available at: <https://github.com/thabeatmjh/STAMBRIDGE>.

**Keywords** EEG-based visual decoding · multimodal contrastive representation learning · spectral–temporal modulation · mid-feature distillation

## 1 Introduction

Decoding visual content from non-invasive brain recordings is a fundamental problem in both cognitive neuroscience and next-generation brain–computer interfaces (BCIs) [1]. Among available neuroimaging modalities, electroencephalography (EEG) is particularly attractive due to its low cost, portability, and high temporal resolution, making it suitable for latency-sensitive applications [2]. Nevertheless, EEG-based visual decoding remains highly challenging because EEG signals inherently exhibit low signal-to-noise ratio (SNR), coarse spatial resolution, and substantial inter-subject variability [3, 4]. For visual decoding, these limitations are further compounded by the modality gap between unstructured brainwaves and highly organized visual–language latent spaces. Consequently, unlike auditory processing where EEG signals natively share temporal alignment with soundwaves, recovering high-level visual semantics from

---

\**Citation:* Jiahe Meng, Weiming Zeng, Yueyang Li, Bo Chai, Hongjie Yan, Zhiguo Zhang, Wai Ting Siok, Nizhuan Wang. STAMBRIDGE: Spectral-Temporal Amplitude-aware Mid-Feature Bridge for EEG Visual Decoding.

EEG requires bridging a massive dimensional and structural divide, making it considerably more difficult than from other neural measurements with higher SNR or finer spatial resolution.

A central prerequisite for EEG-based visual decoding is the extraction of neural representations that simultaneously preserve global temporal context and localized neurophysiological dynamics. Existing temporal modeling paradigms commonly rely on generic sequence architectures, such as the iTransformer [5], which are effective at modeling long-range dependencies but may insufficiently capture localized frequency-aware transients. To incorporate spectral priors, recent studies such as Neural-MCRL [6] introduce frequency-domain modulation mechanisms based on Fast Fourier Transforms (FFT). Although effective in enhancing spectral attention, these methods typically apply hard binary frequency masks before inverse transformations (IFFT). From a signal processing perspective, such abrupt spectral truncation inevitably introduces ringing artifacts in the time domain [7, 8]. The resulting temporal smearing can obscure subtle and short-lived neurophysiological transients that are critical for visual decoding. This issue becomes particularly severe in Rapid Serial Visual Presentation (RSVP) paradigms, where visual stimuli are presented at high frequencies and semantic information is encoded within precise stimulus-locked transient responses. Once these transients are distorted by filtering artifacts, the temporal discriminability between consecutive visual concepts is substantially weakened. To address this, we propose a Spectral-Temporal Amplitude-aware Modulation (STAM) module. Rather than acting as a conventional hard filter, STAM softly integrates spectral priors to extract well-conditioned representations while explicitly preserving the time-domain integrity of neural transients.

Beyond robust EEG representation learning, another major challenge lies in aligning neural embeddings with pretrained vision–language representations such as CLIP (Contrastive Language-Image Pre-training) [9]. As highlighted in recent comprehensive surveys [10], although generative models have significantly advanced visual reconstruction quality, the dominant bottleneck remains the severe modality gap between EEG signals and semantic visual representations [11]. Compared with the semantically structured vision–language embedding space, EEG signals—even after sophisticated encoding—remain only indirectly associated with high-level visual concepts. Existing approaches, including ATM [12] and Neural-MCRL [6], commonly enforce direct one-step alignment between EEG embeddings and vision–language representations. However, this paradigm tightly couples several fundamentally different learning objectives within a single optimization stage, requiring the EEG encoder to simultaneously perform signal denoising, semantic abstraction, and cross-modal geometric alignment. As a consequence, the optimization process becomes dominated by the large gradient updates required for cross-modal matching, which can overwhelm the underlying neural representation learning. This optimization conflict makes it difficult to form a coherent latent structure and often leads to instability and semantic fragmentation, ultimately limiting retrieval and reconstruction performance.

To address aforementioned challenges, we proposed the STAMBRIDGE framework in this paper, whose key contributions are summarized as follows:

- We design an EEG encoding pipeline that combines a Subject-Specific Linear Layer [13, 14], an iTransformer backbone, and the proposed Spectral-Temporal Amplitude-aware Modulation (STAM) module, which integrates multi-scale temporal convolutions and amplitude-derived soft channel weighting to capture frequency-aware transient dynamics while reducing filtering-induced temporal distortion.
- We propose a Mid-Feature Semantic Bridge (MFSB), a model-agnostic alignment module that constructs a regularized intermediate semantic space for staged distillation, thereby alleviating optimization instability caused by the cross-modal gap.
- We evaluate STAMBRIDGE on the THINGS-EEG benchmark, where it achieves competitive zero-shot retrieval performance. Furthermore, qualitative validation using an off-the-shelf latent diffusion model produces semantically coherent image reconstructions, demonstrating the improved alignment quality of the learned representations.

## 2 Related Work

### 2.1 EEG-based Visual Decoding

Visual neural decoding has traditionally relied heavily on functional magnetic resonance imaging (fMRI), whose high-spatial-resolution voxel analysis enables detailed visual reconstruction [15, 16]. However, the low temporal resolution and high operational cost of fMRI limit its practicality for real-time BCIs. EEG has therefore emerged as a promising alternative, offering portability and millisecond-level temporal sensitivity [2]. Early EEG decoding studies mainly focused on coarse categorical classification [17], whereas recent work has shifted toward fine-grained visual retrieval and reconstruction.

To model complex EEG dynamics, recent approaches increasingly use deep sequence backbones, including Transformers and convolutional-attention hybrids like EEG-Conformer [18]. Although these generic encoders provide strong global temporal modeling, they often overlook localized frequency-aware neurophysiological characteristics of EEG, including

transient oscillatory patterns. Moreover, prior attempts to inject spectral priors typically rely on hard frequency masking, which may introduce time-domain ringing artifacts and distort short-lived neural signatures. As a result, learning a well-conditioned neural representation that balances spectral filtering with time-domain integrity remains a central challenge.

The RSVP paradigm has further sharpened this challenge. Unlike block-design settings, where models may exploit low-level statistical cues, RSVP-based datasets such as THINGS-EEG impose stricter constraints on semantic decoding and therefore serve as a more reliable benchmark for evaluating EEG-to-image decoding methods. This setting has motivated recent models to focus on more robust representation learning and cross-modal alignment [19, 20, 6].

## 2.2 Multimodal Contrastive Representation Learning

The emergence of vision–language models such as CLIP has established a robust shared semantic space for multimodal alignment. This paradigm has been adapted to neural decoding by projecting EEG embeddings toward pretrained visual or textual representations through contrastive learning, thereby supporting zero-shot retrieval. Recent zero-shot frameworks, including NICE [20], BraVL [21], ATM [12], and Neural-MCRL [6], have significantly advanced this alignment paradigm. By leveraging contrastive objectives, these methods demonstrate the feasibility of mapping neural time-series signals into high-level semantic manifolds and lay the foundation for modern EEG-to-vision decoding.

## 2.3 Current Cross-Modal Alignment Strategies

To mitigate the aforementioned *modality gap* and the instability of rigid one-step contrastive alignment, recent frameworks have evolved along two distinct trajectories. The first relies on heavy external semantic augmentation, utilizing Retrieval-Augmented Generation (RAG) [22] or Multimodal Large Language Models (MLLMs) [23] to enrich cross-modal supervision. However, these strategies inevitably introduce substantial inference latency and system complexity. The second trajectory focuses on internal alignment mechanisms, such as the Shared Semantic Projector (SSP) and Cognitive Prior Augmentation (CPA) proposed in NeuroBridge [24]. Yet, relying on heavily coupled shared projectors can still propagate optimization pressure directly back to the fragile EEG backbone under low-SNR conditions. These existing limitations highlight the critical need for an internal, decoupled alignment strategy that can buffer optimization instability without relying on computationally expensive external modules.

## 2.4 Generative Prior-based Reconstruction

Recent EEG-to-image decoding methods increasingly rely on latent diffusion models [25] to synthesize detailed visual content from neural signals. Compared with direct pixel-space regression, diffusion-based reconstruction leverages the strong generative priors of pretrained models and has shown promising results in producing visually plausible outputs conditioned on decoded brain representations. This paradigm was pioneered in EEG decoding by methods such as ATM [12], which reformulate brain activity as semantic or textual guidance for image generation.

Recent work has further extended this generative framework to more complex spatial-temporal scenarios, including 3D point cloud generation [26] and cross-task video decoding [27]. Despite these advances in downstream rendering, the generative quality remains fundamentally bottlenecked by the upstream neural representation. Particularly in paradigms characterized by low SNR, such as RSVP, models relying on coarse global conditioning often struggle to preserve fine-grained regional semantics and local structural details [28]. This limitation highlights the importance of extracting well-conditioned EEG embeddings that explicitly preserve localized spectral-temporal transients before applying powerful cross-modal mapping or generative priors.

# 3 Methods

## 3.1 Overview

The objective of STAMBRIDGE is to learn robust EEG representations that bridge the profound gap between low-SNR neural time-series data and highly structured vision–language manifolds (e.g., CLIP space). Let  $\mathcal{D} = \{(\mathbf{X}_i, \mathbf{v}_i, \mathbf{t}_i)\}_{i=1}^N$  denote the dataset of  $N$  samples, where  $\mathbf{X}_i \in \mathbb{R}^{C \times T}$  represents an EEG trial with  $C$  channels and  $T$  time steps, and  $\mathbf{v}_i$  and  $\mathbf{t}_i$  denote the corresponding pretrained visual and textual embeddings.

Although conventional methods encode the raw signal  $\mathbf{X}$  into a latent neural representation (denoted as  $\mathbf{z}_{eeG}$ ), directly enforcing a one-step alignment between  $\mathbf{z}_{eeG}$  and the visual embedding  $\mathbf{v}$  often leads to suboptimal optimization. To address this issue, we adopt a decoupled architecture consisting of two main stages: (1) a tailored EEG Encoder,

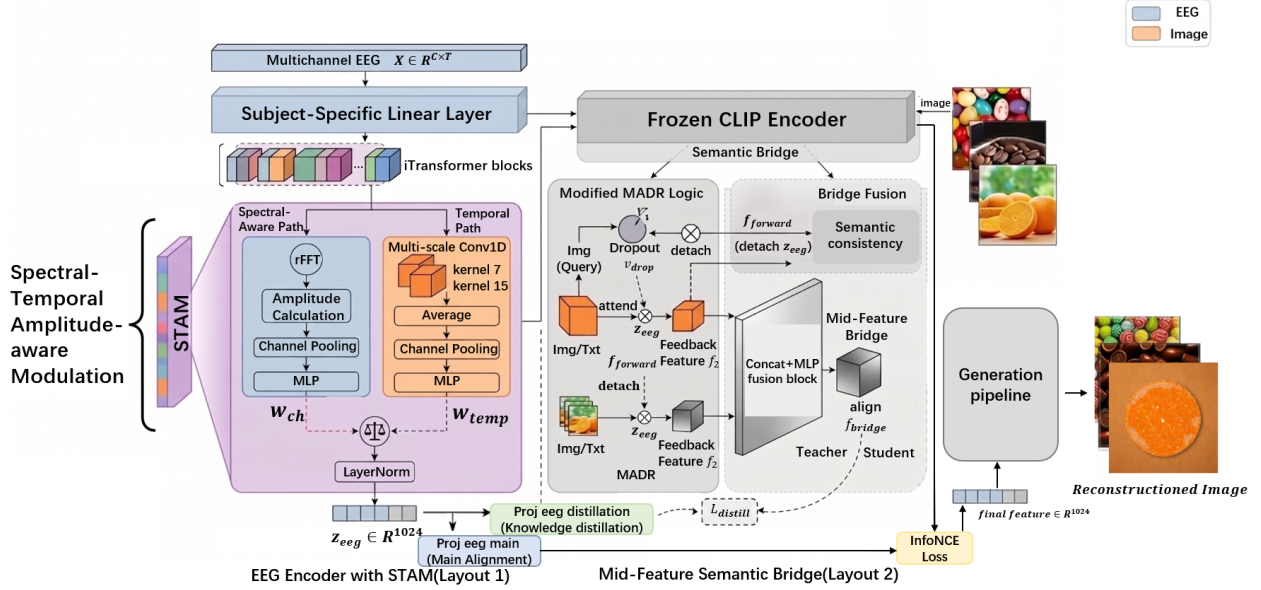


Figure 1: Overall framework of our proposed STAMBRIDGE model, illustrating the Spectral-Temporal Amplitude-aware Modulation (STAM) and the Mid-Feature Semantic Bridge (MFSB).

equipped with **STAM**, designed to extract artifact-suppressed, frequency-aware neural transients that serve as better-conditioned inputs ( $z_{eeeg}$ ); and (2) a model-agnostic **MFSB** that constructs a regularized intermediate space to ease cross-modal alignment via directed routing and staged distillation.

### 3.2 EEG Encoder with Spectral-Temporal Amplitude-aware Modulation

To effectively capture the spatio-temporal dynamics of neural signals and explicitly protect feature integrity, our encoding pipeline strictly follows a specific logic: Multichannel EEG  $\rightarrow$  Subject-Specific Linear Layer  $\rightarrow$  iTransformer blocks  $\rightarrow$  STAM module.

Given a raw EEG trial  $\mathbf{X}_i \in \mathbb{R}^{C \times T}$  with  $C = 63$  channels and  $T = 250$  time steps, the data is first processed by the Subject-Specific Linear Layer. This layer uses pre-calibrated linear projections to map each subject’s channel topology into a shared latent space, thereby mitigating cross-subject spatial variability. The adapted features are then processed by a stack of iTransformer blocks [5] to capture global long-range temporal dependencies.

The resulting sequence is then fed into the STAM. Recent studies indicate that under the extremely low-SNR conditions of rapid visual stimuli (RSVP), aggressive feature truncation can lead to severe feature shift and gradient interference [29, 30]. Therefore, to extract spectral priors without inducing the Gibbs ringing artifacts common in hard-masking inverse fast Fourier transforms (IFFT), STAM employs a soft, decoupled feature extraction strategy. Given the input tensor  $\mathbf{X}_{in} \in \mathbb{R}^{B \times C \times T}$ , it first computes the frequency-domain amplitude along the temporal axis via the real-valued Fast Fourier Transform (rFFT). Instead of masking the spectrum, the mean amplitude serves as a descriptor for a two-layer bottleneck MLP (reduction ratio  $r = 8$ ) with Sigmoid activation, yielding a sample-specific soft channel-weighting matrix  $\mathbf{W}_c \in (0, 1)^{B \times C}$ . This weight is then explicitly broadcasted along the temporal dimension and multiplied element-wise with the original time-domain sequence, maintaining the output dimension of the spectral branch as  $\mathbb{R}^{B \times C \times T}$ .

Simultaneously, to capture transient temporal dynamics, the input sequence is processed by parallel 1D temporal convolutions with distinct receptive fields (kernel sizes  $k \in \{7, 15\}$ ). To preserve the temporal sequence length  $T$ , zero-padding of size  $(k - 1)/2$  is explicitly applied. The multi-scale features are activated via GELU, averaged, and then modulated by a temporal attention mechanism. Specifically, the temporal descriptor is computed via channel-wise mean pooling and passed through a two-layer MLP to generate a sample-specific temporal weight matrix  $\mathbf{W}_t \in (0, 1)^{B \times T}$ , which adaptively scales the sequence along the time axis.

Finally, let  $\mathbf{X}_{spec} \in \mathbb{R}^{B \times C \times T}$  and  $\mathbf{X}_{temp} \in \mathbb{R}^{B \times C \times T}$  denote the modulated outputs from the spectral and temporal branches, respectively. To dynamically balance frequency-aware features and time-domain transients, they are fused via

a learnable weighted addition:

$$\mathbf{X}_{fused} = \lambda_1 \mathbf{X}_{spec} + \lambda_2 \mathbf{X}_{temp}, \quad \text{where } \lambda = \text{Softmax}(\boldsymbol{\alpha}). \quad (1)$$

Here,  $\boldsymbol{\alpha} = [\alpha_1, \alpha_2]^\top \in \mathbb{R}^2$  is a learnable parameter that ensures the sum of fusion weights equals one ( $\lambda_1 + \lambda_2 = 1$ ). To capture local spatial-temporal patterns before semantic projection, the fused output  $\mathbf{X}_{fused}$  is further processed by a shallow convolutional patch embedding module (comprising depthwise/pointwise 2D convolutions and average pooling). It is then flattened and passed through a projection head—comprising sequential Linear, GELU, Dropout, and Layer Normalization layers—to match the  $d = 1024$  dimensional semantic space, yielding  $\mathbf{z}_{eeg} \in \mathbb{R}^d$  as the primary neural representation. Because STAM explicitly avoids hard masking, it preserves critical time-domain transients, a necessity for future tasks requiring regional and spatial semantic control [28].

### 3.3 Mid-Feature Semantic Bridge

To mitigate the instability inherent in direct one-step mapping between  $\mathbf{z}_{eeg}$  and visual semantic spaces, we construct a softened intermediate target using a novel Multi-modal Adaptive Directional Routing (MADR) attention mechanism. Inspired by the success of cross-modal attention in establishing semantic consistency for general image–text matching [31], this design utilizes directed attention to explicitly model how stable semantic modalities interpret the current dynamic neural state, providing a context-aware target for refinement.

#### 3.3.1 Multi-modal Adaptive Directional Routing (MADR)

Standard cross-attention typically treats modalities uniformly. In contrast, MADR dynamically estimates a routing weight matrix to balance visual and textual semantics according to the current state of the neural embedding.

Given a query  $\mathbf{Q}$  from one modality and a set of keys/values  $\{\mathbf{K}_m, \mathbf{V}_m\}_{m=1}^M$  from  $M$  target modalities (e.g., image and text), MADR first computes a head-aware routing probability matrix  $\mathbf{W}_{route} \in \mathbb{R}^{H \times M}$  using a routing multi-layer perceptron (MLP), where  $H$  denotes the number of attention heads:

$$\mathbf{W}_{route} = \text{Softmax}(\text{MLP}_{route}(\text{Pool}(\mathbf{Q}))). \quad (2)$$

Here,  $\text{Pool}(\cdot)$  denotes mean pooling over the token dimension. Specifically, the  $\text{MLP}_{route}$  consists of two linear layers separated by a ReLU activation (with a hidden dimension of 128). For each of the  $H$  attention heads, the MLP generates an  $M$ -dimensional probability distribution ( $M = 2$  for image and text modalities), yielding the  $H \times M$  routing space. This fine-grained design allows each individual head to independently balance its focus between visual and textual semantics. Note that the target visual and textual prototypes ( $\{\mathbf{K}_m, \mathbf{V}_m\}$ ) are pre-extracted using a strictly frozen OpenCLIP ViT-H/14 encoder (pre-trained on the LAION-2B dataset) to ensure a stable reference manifold. To prevent routing collapse during early training, the final linear projection bias is initialized to zero, ensuring an approximately uniform initial routing distribution (i.e.,  $W_{route,i,m} \approx \frac{1}{M}$ ). The resulting routing matrix independently modulates the cross-attention outputs of each individual head (rather than globally per module) before aggregation over modalities. For the  $i$ -th head, the routed attention output is defined as:

$$\mathbf{H}_i = \sum_{m=1}^M W_{route,i,m} \cdot \text{Softmax} \left( \frac{\mathbf{Q}_i \mathbf{K}_{m,i}^\top}{\sqrt{d_k}} \right) \mathbf{V}_{m,i}, \quad (3)$$

where  $W_{route,i,m}$  represents the scalar routing weight corresponding to the  $i$ -th head and  $m$ -th modality (i.e., the  $(i, m)$ -th element of  $\mathbf{W}_{route}$ ). Additionally,  $\mathbf{Q}_i$ ,  $\mathbf{K}_{m,i}$ , and  $\mathbf{V}_{m,i}$  denote the projected query, key, and value matrices specific to the  $i$ -th head, and  $d_k$  is the dimensionality of the head-specific key/query vectors.

#### 3.3.2 Semantic Interaction and Staged Distillation

We employ MADR to construct the regularized Mid-Feature space. Specifically, the neural representation  $\mathbf{z}_{eeg}$  acts as the query to attend to frozen visual and textual prototypes, which serve as the keys and values. This attention mechanism explicitly captures how the current dynamic neural state aligns with and retrieves information from stable semantic modalities. Let  $\mathbf{h}_{attn} \in \mathbb{R}^d$  denote the final aggregated cross-attention output. While MADR aggregates both visual and textual concepts to form a rich semantic context, the final intermediate target must be specifically anchored to the visual modality to optimize for downstream visual decoding tasks. To robustify this representation against low-SNR artifacts and prevent deterministic collapse during training,  $\mathbf{h}_{attn}$  is concatenated with stochastically dropped-out visual features and passed through a fusion network. Formally, the regularized Mid-Feature target, denoted as  $\mathbf{f}_{bridge}$ , is formulated as:

$$\mathbf{f}_{bridge} = \mathcal{N} \left( \text{MLP}_{fuse}([\mathbf{h}_{attn} \parallel \text{Dropout}(\mathbf{v}, p)]) \right), \quad (4)$$

where  $[\cdot \parallel \cdot]$  denotes concatenation along the feature dimension,  $\mathbf{v}$  is the target visual prototype, and  $\text{Dropout}(\cdot, p)$  applies stochastic masking with probability  $p$  (empirically set to 0.4). The fusion network  $\text{MLP}_{fuse}$  consists of Layer Normalization, linear projections, and GELU activations, while  $\mathcal{N}(\cdot)$  represents strictly enforced L2-normalization. The resulting output  $\mathbf{f}_{bridge}$  serves as the context-aware, softened target for the subsequent staged distillation.

Unlike raw visual embeddings,  $\mathbf{f}_{bridge}$  is deeply conditioned on the neural context and therefore provides a smoother optimization target. During training, we adopt a **staged distillation** strategy formulated as a multi-task objective. First, to maintain global semantic consistency, the primary EEG embedding  $\mathbf{z}_{eeg}$  is directly aligned with the visual semantic manifold via the InfoNCE loss [32]:

$$\mathcal{L}_{main} = \mathcal{L}_{\text{InfoNCE}}(\mathbf{z}_{eeg}, \mathbf{v}). \quad (5)$$

Simultaneously, the intermediate bridge is anchored to the target visual semantic manifold:

$$\mathcal{L}_{bridge} = \mathcal{L}_{\text{InfoNCE}}(\mathbf{f}_{bridge}, \mathbf{v}). \quad (6)$$

Finally, an auxiliary projection of the EEG embedding is distilled toward this aligned intermediate representation. To stabilize optimization and avoid degenerate coupling,  $\mathbf{f}_{bridge}$  is detached from the computation graph during distillation:

$$\mathcal{L}_{distill} = \mathcal{L}_{\text{InfoNCE}}(\text{Proj}(\mathbf{z}_{eeg}), \mathbf{f}_{bridge}^{\text{detach}}). \quad (7)$$

Here,  $\text{Proj}(\cdot)$  denotes an auxiliary projection head with stabilized residual initialization and orthogonal weights to prevent gradient interference. The total objective integrates these components:

$$\mathcal{L}_{total} = \lambda_0 \mathcal{L}_{main} + \lambda_1 \mathcal{L}_{bridge} + \lambda_2 \mathcal{L}_{distill}. \quad (8)$$

The latent representations ( $\mathbf{f}_{bridge}, \mathbf{v}, \mathbf{z}_{eeg}$ ) are strictly  $\ell_2$ -normalized within the unified  $d = 1024$  space. The InfoNCE objectives follow a symmetric formulation parameterized by a learnable temperature  $\tau$ . To ensure a smooth transition from global alignment to fine-grained distillation, we empirically set  $\lambda_0 = 0.99$ ,  $\lambda_1 = 0.5$ , while linearly warming up  $\lambda_2$  from 0.0 to 0.2 across epochs. This explicit staged optimization acts as a buffer against the modality gap without interfering with the main feature extraction path.

## 4 Experiments

### 4.1 Experimental Setup

**Dataset and Preprocessing** We evaluate our framework on the THINGS-EEG dataset [19], a large-scale benchmark containing EEG recordings from 10 subjects during the RSVP of natural images sourced from the THINGS database [33]. The dataset comprises 16,540 training image concepts and 200 distinct test concepts. Following standard protocols, the continuous EEG data is segmented into trials from 0 to 1000 ms relative to stimulus onset, baseline-corrected, and downsampled to 250 Hz, resulting in 63-channel sequence inputs.

**Implementation Details** All experiments were conducted on a workstation equipped with a single NVIDIA RTX 3090 GPU (24GB VRAM), an Intel Xeon Platinum 8474C CPU, and 80GB of RAM. Because our architecture constructs an internal MFSB rather than relying on massive external VLMs or RAG databases [22, 34], the framework is highly memory-efficient and well suited for single-GPU iterative training. All experiments were repeated using three random seeds. During the contrastive alignment phase, models were optimized using the AdamW optimizer with a base learning rate of  $3 \times 10^{-4}$  and a batch size of 512 for 40 epochs. For qualitative generative validation, we adopt the two-stage generation framework established by ATM [12]. First, a Diffusion Prior translates the bridged EEG representations into intermediate visual embeddings using 50 DDIM steps with a classifier-free guidance scale of 5.0. Subsequently, these intermediate embeddings are fed into an IP-Adapter [35] to condition a stable diffusion model for final image synthesis. To accelerate decoding, this second stage was optimized to require only 4 inference steps, significantly reducing computational overhead without sacrificing visual fidelity.

**Evaluation Metrics** As the primary objective is to evaluate cross-modal semantic alignment, we report Top-1 and Top-5 accuracy in a 200-way zero-shot image retrieval setting. For the downstream qualitative image generation task, we adopt standard high-level semantic metrics—including AlexNet(2), AlexNet(5), InceptionV3, CLIP similarity, and SwAV—to quantitatively assess the semantic consistency between the generated images and the ground-truth visual stimuli.

### 4.2 Zero-Shot Image Retrieval Results

We compare STAMBRIDGE against recent EEG-based visual decoding models, including BraVL [21], NICE [20], MB2C [36], ATM [12], and Neural-MCRL [6]. Table 1 presents the subject-dependent 200-way zero-shot retrieval accuracy across all 10 subjects.

Table 1: Overall 200-way zero-shot retrieval accuracy (%) on the THINGS-EEG dataset (Subject-Dependent). Results are reported as mean  $\pm$  std across 10 subjects.

Method	S1		S2		S3		S4		S5		S6		S7		S8		S9		S10		Mean $\pm$ Std	
	T1	T5	T1	T5	T1	T5	T1	T5	T1	T5	T1	T5	T1	T5	T1	T5	T1	T5	T1	T5	T1	T5
BraVL	6.1	17.9	4.9	14.9	5.6	17.4	4.9	15.1	4.0	13.4	6.0	18.1	6.5	20.3	8.8	23.7	4.3	13.9	7.0	13.7	5.81 $\pm$ 1.42	16.84 $\pm$ 3.32
NICE	11.5	32.0	12.5	35.5	12.5	41.5	18.5	48.0	9.5	28.5	15.0	42.5	16.0	41.0	19.5	51.0	16.5	37.5	16.5	43.5	14.80 $\pm$ 3.21	40.10 $\pm$ 6.91
MB2C	23.0	56.0	23.0	56.0	30.0	61.5	21.5	48.5	21.5	48.5	32.0	61.5	28.5	59.5	40.5	70.0	27.5	59.0	29.5	69.0	27.70 $\pm$ 5.89	58.95 $\pm$ 7.24
ATM	23.0	48.0	19.5	42.5	33.0	58.5	29.5	57.0	26.5	46.5	25.5	61.0	28.5	59.5	40.5	71.0	30.0	53.0	37.5	66.5	29.35 $\pm$ 6.37	56.35 $\pm$ 8.97
Neural-MCRL	28.5	56.5	25.5	56.5	30.0	59.0	34.0	62.0	24.0	51.0	27.0	56.5	30.5	58.5	42.5	76.5	30.5	53.5	38.0	67.0	31.05 $\pm$ 5.71	59.70 $\pm$ 7.36
<b>STAMBRIDGE (Ours)</b>	<b>33.0</b>	<b>67.5</b>	<b>31.5</b>	<b>64.0</b>	<b>36.0</b>	<b>66.5</b>	<b>37.0</b>	<b>67.5</b>	<b>25.5</b>	<b>58.0</b>	<b>29.5</b>	<b>62.5</b>	<b>33.5</b>	<b>63.0</b>	<b>48.5</b>	<b>79.0</b>	<b>32.5</b>	<b>61.0</b>	<b>38.0</b>	<b>70.5</b>	<b>34.50 <math>\pm</math> 6.14</b>	<b>65.95 <math>\pm</math> 5.85</b>

Table 2: Cross-model generalization of the Mid-Feature Semantic Bridge. Integrating the bridge consistently improves both Top-1 and Top-5 accuracy across different baseline architectures. Results are reported as mean  $\pm$  std across 10 subjects.

Model Configuration	Top-1 (%)	Top-5 (%)
NICE (Baseline)	14.80 $\pm$ 3.21	40.10 $\pm$ 6.91
<b>NICE + MFSB</b>	<b>15.40 <math>\pm</math> 3.89</b> (+0.60)	<b>42.70 <math>\pm</math> 4.82</b> (+2.60)
ATM (Baseline)	29.35 $\pm$ 6.37	56.35 $\pm$ 8.97
<b>ATM + MFSB</b>	<b>30.55 <math>\pm</math> 5.11</b> (+1.20)	<b>61.35 <math>\pm</math> 7.58</b> (+5.00)
Neural-MCRL (Baseline)	31.05 $\pm$ 5.71	59.70 $\pm$ 7.36
<b>Neural-MCRL + MFSB</b>	<b>32.75 <math>\pm</math> 4.91</b> (+1.60)	<b>62.70 <math>\pm</math> 5.87</b> (+3.00)

Table 3: Ablation study on the core components in STAMBRIDGE. Accuracy is averaged across 10 subjects on the 200-way zero-shot retrieval task. Results are reported as mean  $\pm$  std across 10 subjects.

Model Configuration	Top-1 (%)	Top-5 (%)
Baseline (Neural-MCRL)	31.05 $\pm$ 5.71	59.70 $\pm$ 7.36
+ STAM Only	33.95 $\pm$ 5.19	63.60 $\pm$ 6.66
+ MFSB Only	32.75 $\pm$ 4.91	62.70 $\pm$ 5.87
<b>STAMBRIDGE (Ours)</b>	<b>34.50 <math>\pm</math> 6.14</b>	<b>65.95 <math>\pm</math> 5.85</b>

STAMBRIDGE achieves an average Top-1 accuracy of 34.50% and a Top-5 accuracy of 65.95%, establishing a strong result on this benchmark. Compared to the strong baseline (Neural-MCRL), STAMBRIDGE provides an absolute improvement of +3.45% in Top-1 and +6.25% in Top-5 accuracy. These improvements highlight the effectiveness of our decoupled design, in which STAM provides explicit spectral-temporal priors to produce better-conditioned neural representations and a semantic bridge that smooths the cross-modal alignment trajectory. The notable gain in Top-5 accuracy suggests that our method helps regularize the latent space, clustering semantically related concepts even when finding the single correct match is challenging.

### 4.3 Model-Agnostic Generality of Semantic Bridge

To explicitly validate the plug-and-play nature of the proposed Mid-Feature Semantic Bridge, we integrate it as an independent module into three distinct baseline architectures: NICE [20], ATM [12], and Neural-MCRL [6]. We evaluate the average 200-way zero-shot retrieval accuracy across all subjects under identical experimental settings.

As shown in Table 2, the integration of the semantic bridge consistently improves retrieval performance across all tested models. Notably, the bridge yields substantial increases in Top-5 accuracy (+2.60% for NICE, +5.00% for ATM, and +3.00% for Neural-MCRL). This consistent enhancement across different sequence encoders suggests that the staged distillation process can mitigate brittle optimization under the evaluated settings. By providing a regularized intermediate target, the bridge supports a robust alignment trajectory regardless of the underlying EEG feature extractor.

### 4.4 Ablation Studies: Disentangling Module Contribution

To systematically evaluate the individual contributions of the STAM and MFSB within our full framework, we conducted ablation studies under identical training conditions. The average retrieval results are summarized in Table 3.

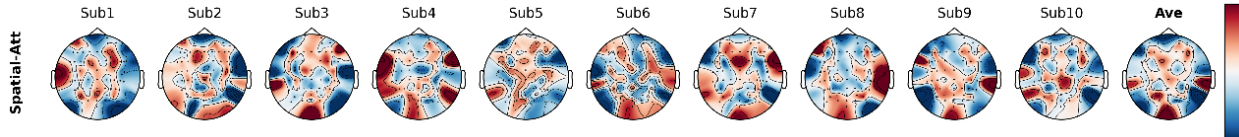


Figure 2: Visualization of the learned spatial attention maps across 10 subjects (Sub1–Sub10) and their grand average (Ave). The activation heatmaps consistently highlight the occipital and parietal regions, confirming that the model captures biologically meaningful visual processing signals rather than noise.

When adding only STAM to the baseline, the Top-1 accuracy increases by 2.90%. This indicates that explicitly capturing spectral-temporal transients without introducing masking artifacts provides a useful inductive bias for precise semantic discrimination.

Conversely, treating the semantic bridge as a plug-and-play extension and integrating it independently yields a modest Top-1 improvement (+1.70%) but provides a larger increase in Top-5 accuracy (+3.90%). This observation aligns perfectly with the cross-model findings in Table 2, further supporting that staged distillation helps mitigate brittle optimization. Combining both modules yields complementary benefits, extracting better-conditioned features (via STAM) that are more effectively routed and aligned (via the MFSB).

#### 4.5 Qualitative Validation and Visualization

To further validate the structural integrity of the learned EEG embeddings, we perform visual reconstruction and latent space analysis.

**Neurophysiological Interpretability via Spatial Attention** To verify reliance on biologically meaningful signals, we visualize the EEG encoder’s spatial attention weights (Fig. 2). The activation maps across all 10 subjects and their grand average (Ave) demonstrate a strong, consistent focus on occipital and parietal regions, aligning with the neurophysiological basis of human visual processing. This consistency validates that our Subject-Specific Linear Layer and STAM effectively mitigate spatial variance while preserving task-relevant cues before cross-modal alignment.

**Cross-Modal Latent Space Alignment** To intuitively understand the effectiveness of our MFSB, we visualize the learned feature representations using t-SNE (Fig. 3). The visualization reveals that the EEG features exhibit clustering patterns that correspond to the underlying visual semantics, indicating improved intra-class compactness and inter-class separability.

**Zero-Shot Retrieval Visualization** As shown in the Top-10 zero-shot retrieval results (Fig. 4), given an unseen EEG query, the model retrieves images that generally share the same high-level semantic category. Even when the Top-1 result is not the target image, the subsequent retrieved candidates remain semantically consistent, often preserving the shape, color palette, and object category. This clustering behavior is consistent with the substantial improvement in our Top-5 retrieval accuracy.

**Semantic Image Reconstruction via Generative Prior** Previous visual decoding methods typically rely on complex, dual-pathway generators that combine both low-level (pixel-space) and high-level (semantic) pipelines to synthesize images. However, recovering deterministic low-level visual features from noisy EEG signals is exceptionally challenging and often leads to overfitting [12]. In this work, following the semantic-prompting philosophy established by ATM [12], we treat the generative pipeline not as the primary reconstruction objective, but strictly as a qualitative validation tool for our latent space. Therefore, we deliberately omit the easy-to-overfit low-level pipeline and feed our bridged MFSB representations exclusively into the high-level semantic generation pipeline (i.e., mapping to intermediate embeddings via a Diffusion Prior, followed by rendering via an IP-Adapter conditioned diffusion model). By doing so, we observe that robust latent alignment alone is sufficient to drive coherent image synthesis. This qualitative outcome suggests that our learned representations successfully capture the necessary semantic structures, demonstrating that when the cross-modal semantic bridge is sufficiently optimized, visual decoding can be achieved without the necessity of engineering heavily coupled, dual-pathway pixel regression architectures.

Table 4 presents a concise quantitative comparison of generative performance, focusing strictly on high-level semantic indicators. Our model yields constrained performance on low-level structural metrics (e.g., SSIM) compared to ATM [12]. This is expected, as we explicitly omit the spatial regression branch to prevent overfitting. However, the true measure of latent cognitive alignment relies on high-level semantics. As shown in Table 4, STAMBRIDGE demonstrates

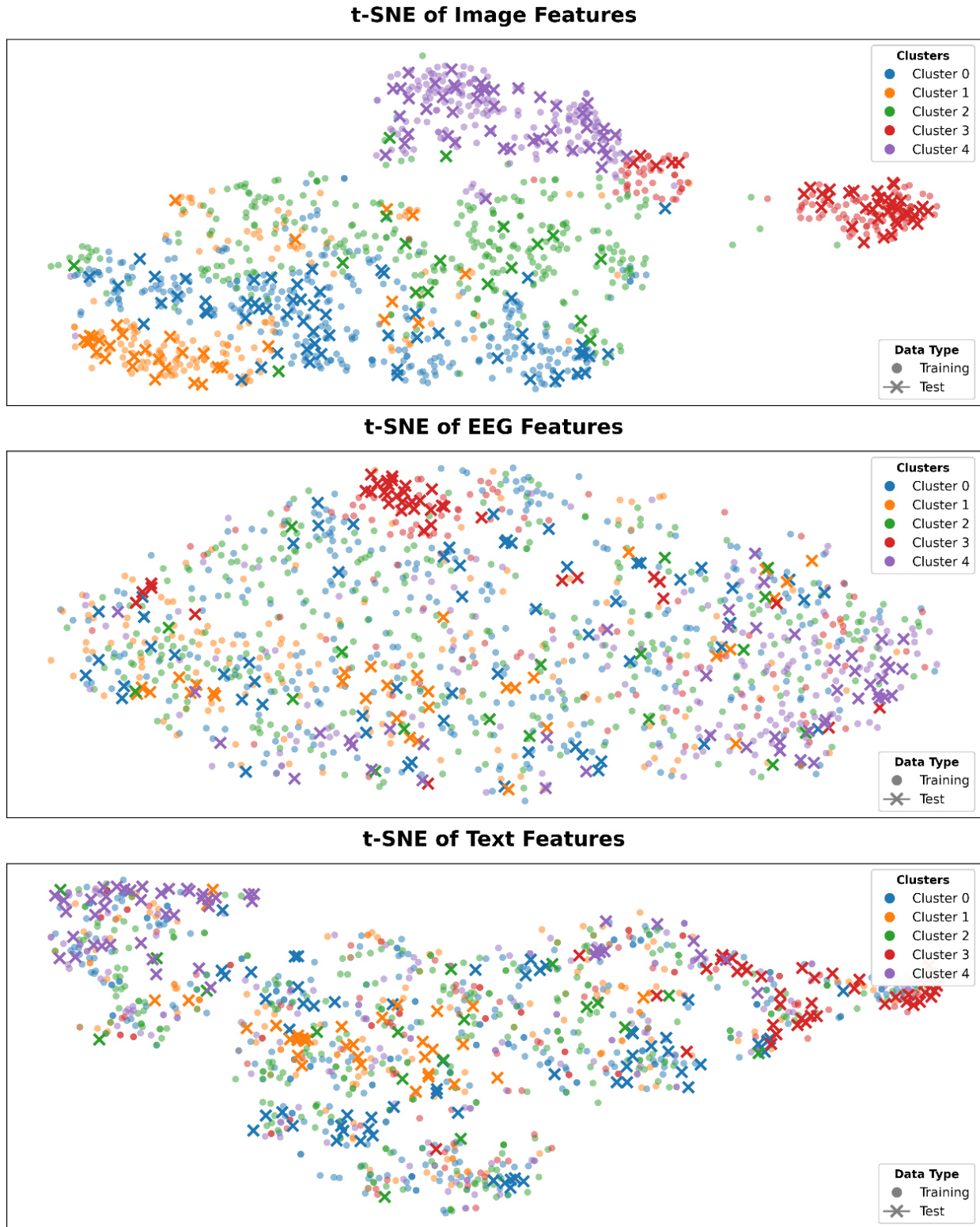


Figure 3: t-SNE visualization of Image, EEG, and Text features. STAMBRIDGE successfully aligns EEG features into semantically consistent clusters that correspond closely to the visual and textual manifolds.

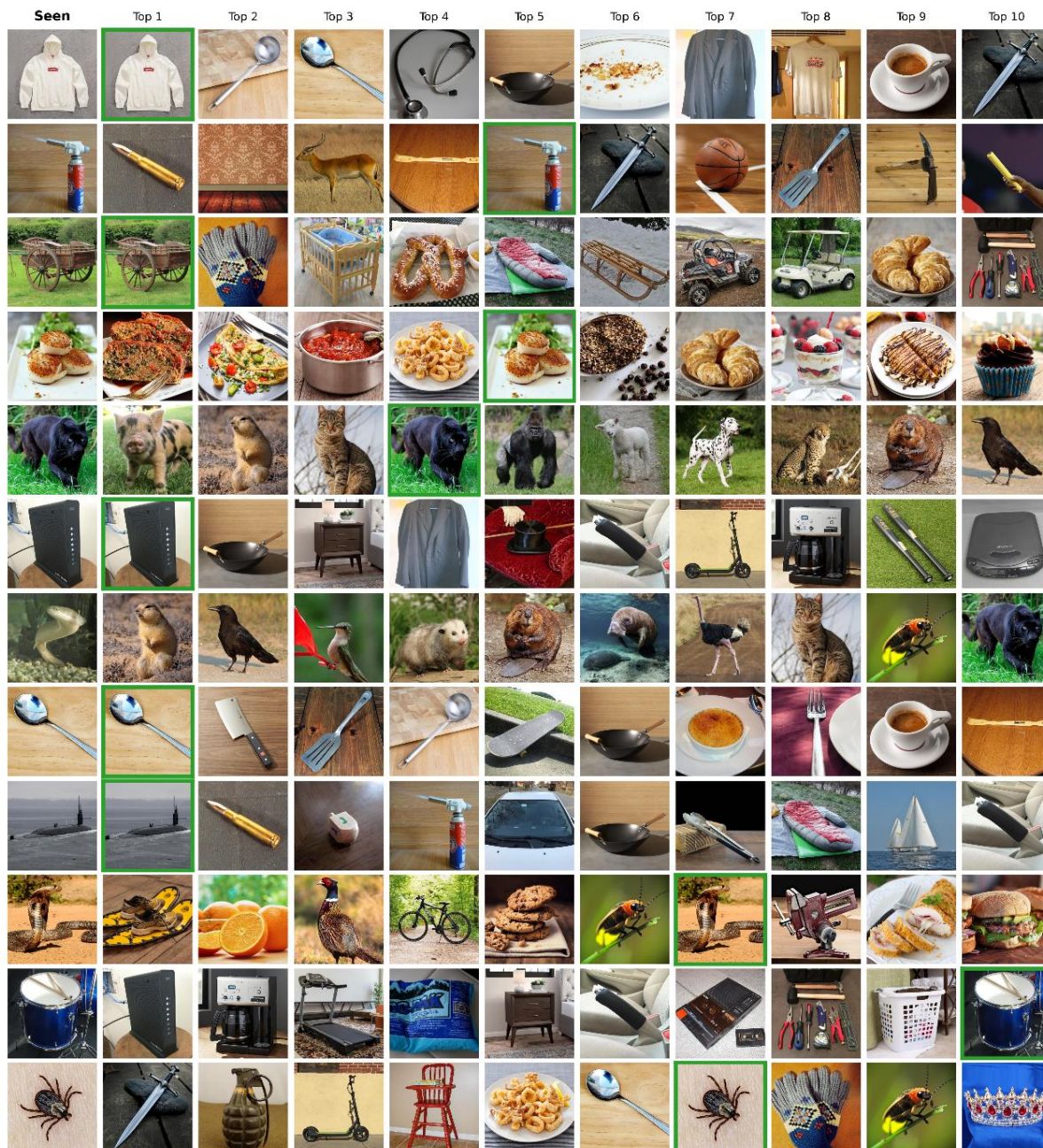


Figure 4: Top-10 zero-shot image retrieval results based on unseen EEG queries. The green boxes indicate correct matches (Top-1). Even for incorrect Top-1 retrievals, the subsequent candidates exhibit highly consistent semantics, demonstrating the robustness of our learned representations.

a substantial lead across major deep semantic metrics when compared to ATM (on Sub-08) and the single-modality baseline CognitionCatcher [37]. Figure 5 presents representative qualitative reconstructions. Additional qualitative reconstruction results for the remaining subjects are provided in the Appendix (Section A).

Table 4: Quantitative comparison of generative performance across all subjects. Our framework yields competitive or superior high-level semantic metrics (AlexNet, Inception, SwAV) compared to state-of-the-art baselines. Results for STAMBRIDGE are reported as mean  $\pm$  std across 10 subjects.

Subject / Method	PixCorr $\uparrow$	SSIM $\uparrow$	AlexNet(2) $\uparrow$	AlexNet(5) $\uparrow$	Inception $\uparrow$	CLIP $\uparrow$	EffNet-B $\uparrow$	SwAV $\downarrow$
Sub-01	0.119	0.335	0.789	0.863	0.698	0.724	0.897	0.526
Sub-02	0.146	0.321	0.803	0.852	0.716	0.734	0.893	0.531
Sub-03	0.145	0.282	0.773	0.857	0.736	0.739	0.891	0.514
Sub-04	0.122	0.325	0.786	0.894	0.775	0.788	0.864	0.487
Sub-05	0.115	0.341	0.791	0.822	0.673	0.670	0.905	0.538
Sub-06	0.160	0.289	0.801	0.861	0.697	0.702	0.903	0.545
Sub-07	0.117	0.283	0.767	0.869	0.694	0.747	0.882	0.524
Sub-08	0.159	0.304	0.802	0.879	0.765	0.759	0.861	0.502
Sub-09	0.121	0.281	0.732	0.825	0.673	0.674	0.897	0.548
Sub-10	0.131	0.345	0.798	0.876	0.741	0.763	0.871	0.477
Mean $\pm$ Std Performance Comparison								
CognitionCapturer (Image) [37]	0.132	<b>0.321</b>	<b>0.813</b>	0.671	0.664	0.705	-	0.599
<b>STAMBRIDGE</b>	<b>0.134 <math>\pm</math> 0.018</b>	<b>0.311 <math>\pm</math> 0.026</b>	<b>0.784 <math>\pm</math> 0.022</b>	<b>0.860 <math>\pm</math> 0.023</b>	<b>0.717 <math>\pm</math> 0.036</b>	<b>0.730 <math>\pm</math> 0.038</b>	<b>0.886 <math>\pm</math> 0.016</b>	<b>0.519 <math>\pm</math> 0.024</b>
Subject-08 Specific Comparison								
ATM (Sub-08 Only) [12]	-	<b>0.345</b>	0.776	0.866	0.734	<b>0.786</b>	-	0.582
<b>STAMBRIDGE (Sub-08)</b>	<b>0.159</b>	0.304	<b>0.802</b>	<b>0.879</b>	<b>0.765</b>	0.759	<b>0.861</b>	<b>0.502</b>



Figure 5: Qualitative results of semantic image reconstruction across different subjects. Each subject shows the Best, Median, and Worst reconstruction cases based on semantic similarity.

## 5 Discussion

### 5.1 Backbone Integrity vs. Aggressive End-to-End Alignment

Unlike fMRI, EEG suffers from severe spatial smearing (the Volume Conduction Effect [1]), making pixel-level reconstruction ill-posed. Consequently, when prior works attempt aggressive end-to-end regression between EEG and spatial latents, the network often encounters *Spatial Mean Collapse*.

Furthermore, under the RSVP paradigm, EEG signals exhibit exceptionally low SNR. As indicated by recent works [29, 30], forcing highly coupled end-to-end alignment can destroy the original neural features. Our pipeline sequence—Multichannel EEG, Subject-specific layer, iTransformer, and STAM—explicitly prioritizes the preservation of the neural backbone. STAM ensures that transient temporal dynamics are not washed out by hard-masking, providing a rich, uncorrupted foundation for the subsequent semantic bridge.

### 5.2 Internal Bridging vs. Heavy External Dependencies

To bypass direct regression limitations, the field increasingly treats EEG as a *semantic prompt*. However, aligning this prompt with visual space often relies on heavy external dependencies like RAG [22] or MLLMs [23]. While effective, these shift the computational burden to external pipelines, hindering iterative training and real-time edge deployment. In contrast, our internal MFSB architecture achieves robust alignment purely through optimized staged distillation, without introducing the latency and memory overhead associated with these heavy external modules.

### 5.3 Limitations and Future Work

While STAMBRIDGE yields significant advantages in stability, challenges remain for real-world deployment. First, transferring a pre-trained visual decoder to an unseen subject without calibration is hindered by extreme inter-subject

EEG variability [13]. Future work will explore subject-invariant representation learning, such as domain adaptation [14], to align neural manifolds across individuals. Second, despite accelerating the spatial rendering phase to merely 4 inference steps, the reliance on a 50-step Diffusion Prior inversion still incurs computational latency. Future iterations will explore direct one-step distillation models to achieve millisecond-level closed-loop generative decoding without sacrificing structural fidelity.

## 6 Conclusion

We propose STAMBRIDGE, a versatile framework for EEG-based visual decoding that moves beyond brittle, one-step alignments toward richer, context-aware multimodal representations. It features a tailored EEG encoding pipeline with a Spectral-Temporal Amplitude-aware Modulation (STAM) that uses soft channel weighting and multi-scale temporal convolutions to preserve frequency-aware transients without time-domain masking artifacts. Building on this, we introduce a Mid-Feature Semantic Bridge (MFSB) that dynamically constructs a regularized intermediate space, easing cross-modal alignment via staged distillation while preserving the primary feature extraction path.

Empirically, STAMBRIDGE achieves competitive zero-shot retrieval performance on the THINGS-EEG benchmark (34.50% Top-1, 65.95% Top-5 accuracy). Extensive ablation studies confirm that our semantic bridge acts as an effective plug-and-play module to improve optimization stability and candidate coverage. While cross-subject generalization remains a future challenge, our framework provides a promising foundation for semantically aligned EEG representation learning.

## References

- [1] Yueyang Li, Weiming Zeng, Wenhao Dong, Di Han, Lei Chen, Hongyu Chen, Zijian Kang, Shengyu Gong, Hongjie Yan, Wai Ting Siok, et al. A tale of single-channel electroencephalogram: Devices, datasets, signal processing, applications, and future directions. *IEEE Transactions on Instrumentation and Measurement*, pages 1–20, 2025.
- [2] Francis R Willett, Donald T Avansino, Leigh R Hochberg, Jaimie M Henderson, and Krishna V Shenoy. High-performance brain-to-text communication via handwriting. *Nature*, 593(7858):249–254, 2021.
- [3] Erin Gibson, Nancy J Lobaugh, Steve Joordens, and Anthony R McIntosh. Eeg variability: Task-driven or subject-driven signal of interest? *NeuroImage*, 252:119034, 2022.
- [4] Lichao Xu, Minpeng Xu, Yufeng Ke, Xingwei An, Shuang Liu, and Dong Ming. Cross-dataset variability problem in eeg decoding with deep learning. *Frontiers in human neuroscience*, 14:103, 2020.
- [5] Yong Liu, Tengge Hu, Haoran Zhang, Haixu Wu, Shiyu Wang, Lintao Ma, and Mingsheng Long. itransformer: Inverted transformers are effective for time series forecasting. In *International conference on learning representations*, volume 2024, pages 11116–11140, 2024.
- [6] Yueyang Li, Zijian Kang, Shengyu Gong, Wenhao Dong, Weiming Zeng, Hongjie Yan, Wai Ting Siok, and Nizhuan Wang. Neural-mcrl: Neural multimodal contrastive representation learning for eeg-based visual decoding. In *2025 IEEE International Conference on Multimedia and Expo (ICME)*, pages 1–6. IEEE, 2025.
- [7] Andreas Widmann and Erich Schröger. Filter effects and filter artifacts in the analysis of electrophysiological data. *Frontiers in psychology*, 3:233, 2012.
- [8] Andreas Widmann, Erich Schröger, and Burkhard Maess. Digital filter design for electrophysiological data—a practical approach. *Journal of neuroscience methods*, 250:34–46, 2015.
- [9] Alec Radford, Jong Wook Kim, Chris Hallacy, Aditya Ramesh, Gabriel Goh, Sandhini Agarwal, Girish Sastry, Amanda Askell, Pamela Mishkin, Jack Clark, et al. Learning transferable visual models from natural language supervision. In *International conference on machine learning*, pages 8748–8763. PmLR, 2021.
- [10] Wei Li, Penglu Zhao, Cheng Xu, Yingting Hou, Wenhao Jiang, and Aiguo Song. Deep learning for eeg-based visual classification and reconstruction: Panorama, trends, challenges and opportunities. *IEEE Transactions on Biomedical Engineering*, 72(11):3374–3390, 2025.
- [11] Sedigheh Eslami and Gerard de Melo. Mitigate the gap: Investigating approaches for improving cross-modal alignment in clip. *arXiv preprint arXiv:2406.17639*, 2024.
- [12] Dongyang Li, Chen Wei, Shiyong Li, Jiachen Zou, and Quanying Liu. Visual decoding and reconstruction via eeg embeddings with guided diffusion. *Advances in Neural Information Processing Systems*, 37:102822–102864, 2024.

- [13] Dongrui Wu, Xue Jiang, and Ruimin Peng. Transfer learning for motor imagery based brain–computer interfaces: A tutorial. *Neural Networks*, 153:235–253, 2022.
- [14] Jinpeng Li, Shuang Qiu, Changde Du, Yixin Wang, and Huiguang He. Domain adaptation for eeg emotion recognition based on latent representation similarity. *IEEE Transactions on Cognitive and Developmental Systems*, 12(2):344–353, 2019.
- [15] Paul Scotti, Atmadeep Banerjee, Jimmie Goode, Stepan Shabalin, Alex Nguyen, Aidan Dempster, Nathalie Verlinde, Elad Yundler, David Weisberg, Kenneth Norman, et al. Reconstructing the mind’s eye: fmri-to-image with contrastive learning and diffusion priors. *Advances in Neural Information Processing Systems*, 36:24705–24728, 2023.
- [16] Yu Takagi and Shinji Nishimoto. High-resolution image reconstruction with latent diffusion models from human brain activity. In *Proceedings of the IEEE/CVF conference on computer vision and pattern recognition*, pages 14453–14463, 2023.
- [17] Tijl Grootswagers, Amanda K Robinson, and Thomas A Carlson. The representational dynamics of visual objects in rapid serial visual processing streams. *NeuroImage*, 188:668–679, 2019.
- [18] Yonghao Song, Qingqing Zheng, Bingchuan Liu, and Xiaorong Gao. Eeg conformer: Convolutional transformer for eeg decoding and visualization. *IEEE Transactions on Neural Systems and Rehabilitation Engineering*, 31:710–719, 2022.
- [19] Alessandro T Gifford, Kshitij Dwivedi, Gemma Roig, and Radoslaw M Cichy. A large and rich eeg dataset for modeling human visual object recognition. *NeuroImage*, 264:119754, 2022.
- [20] Yonghao Song, Bingchuan Liu, Xiang Li, Nanlin Shi, Yijun Wang, and Xiaorong Gao. Decoding natural images from eeg for object recognition. In *International conference on learning representations*, volume 2024, pages 47648–47665, 2024.
- [21] Changde Du, Kaicheng Fu, Jinpeng Li, and Huiguang He. Decoding visual neural representations by multimodal learning of brain-visual-linguistic features. *IEEE Transactions on Pattern Analysis and Machine Intelligence*, 45(9):10760–10777, 2023.
- [22] Jun-Mo Kim, Woohyeok Choi, Sang-Jun Park, Keun-Soo Heo, Young-Han Son, Ji-Hye Oh, Dong-Hee Shin, and Tae-Eui Kam. Seeeg: Semantic-aware eeg-based multi-modal retrieval-augmented generation for high-fidelity visual brain decoding. In *Proceedings of the IEEE/CVF International Conference on Computer Vision*, pages 4824–4833, 2025.
- [23] Chengjian Xu, Yonghao Song, Qiong Wang, and Qingqing Zheng. Mindsae: Advancing semantic perception for m/eeg-based visual decoding via unified multimodal alignment framework. *Biomedical Signal Processing and Control*, 123:110390, 2026.
- [24] Wenjiang Zhang, Sifeng Wang, Yuwei Su, Xinyu Li, Chen Zhang, and Suyu Zhong. Neurobridge: Bio-inspired self-supervised eeg-to-image decoding via cognitive priors and bidirectional semantic alignment. In *Proceedings of the AAAI Conference on Artificial Intelligence*, volume 40(21), pages 18028–18036, 2026.
- [25] Robin Rombach, Andreas Blattmann, Dominik Lorenz, Patrick Esser, and Björn Ommer. High-resolution image synthesis with latent diffusion models. In *Proceedings of the IEEE/CVF conference on computer vision and pattern recognition*, pages 10684–10695, 2022.
- [26] Zhanqiang Guo, Jiamin Wu, Yonghao Song, Jiahui Bu, Weijian Mai, Qihao Zheng, Wanli Ouyang, and Chunfeng Song. Neuro-3d: Towards 3d visual decoding from eeg signals. In *Proceedings of the Computer Vision and Pattern Recognition Conference*, pages 23870–23880, 2025.
- [27] Shuai Huang, Huan Luo, Haodong Jing, Qixian Zhang, Litao Chang, Yating Feng, Xiao Lin, Chendong Qin, Han Chen, Shuwen Jia, et al. Need: Cross-subject and cross-task generalization for video and image reconstruction from eeg signals. *Advances in Neural Information Processing Systems*, 38:173134–173173, 2026.
- [28] Xin Xiang, Wenhui Zhou, Haonan Zhu, Yunrui Li, Guojun Dai, and Lili Lin. Eeg-driven natural image reconstruction with regional semantic awareness. *Pattern Recognition*, 172:112589, 2026.
- [29] Daowen Xiong, Liangliang Hu, Jiahao Jin, Yikang Ding, Congming Tan, Jing Zhang, and Yin Tian. Interpretable cross-modal alignment network for eeg visual decoding with algorithm unrolling. *IEEE Transactions on Neural Networks and Learning Systems*, 36(11):19894–19908, 2025.
- [30] Wenxuan Ma, Hongxin Zhang, Yexuan Li, and Mingyi Wei. Neurodecoder: A new framework for image decoding and reconstruction of eeg signals. *IEEE Journal of Biomedical and Health Informatics*, pages 1–14, 2026.
- [31] Xing Xu, Tan Wang, Yang Yang, Lin Zuo, Fumin Shen, and Heng Tao Shen. Cross-modal attention with semantic consistence for image–text matching. *IEEE transactions on neural networks and learning systems*, 31(12):5412–5425, 2020.

- [32] Aaron van den Oord, Yazhe Li, and Oriol Vinyals. Representation learning with contrastive predictive coding. *arXiv preprint arXiv:1807.03748*, 2018.
- [33] Martin N Hebart, Adam H Dickter, Alexis Kidder, Wan Y Kwok, Anna Corriveau, Caitlin Van Wicklin, and Chris I Baker. Things: A database of 1,854 object concepts and more than 26,000 naturalistic object images. *PloS one*, 14(10):e0223792, 2019.
- [34] H Jing, Y Ma, P Yang, H Li, S Huang, B Chen, and N Zheng. Damind: Zero-shot visual cross-domain alignment and representation for eeg decoding. *IEEE Transactions on Image Processing: a Publication of the IEEE Signal Processing Society*, 35:3214–3227, 2026.
- [35] Hu Ye, Jun Zhang, Sibio Liu, Xiao Han, and Wei Yang. Ip-adapter: Text compatible image prompt adapter for text-to-image diffusion models. *arXiv preprint arXiv:2308.06721*, 2023.
- [36] Yayun Wei, Lei Cao, Hao Li, and Yilin Dong. Mb2c: Multimodal bidirectional cycle consistency for learning robust visual neural representations. In *Proceedings of the 32nd ACM International Conference on Multimedia*, pages 8992–9000, 2024.
- [37] Kaifan Zhang, Lihuo He, Xin Jiang, Wen Lu, Di Wang, and Xinbo Gao. Cognitioncapturer: Decoding visual stimuli from human eeg signal with multimodal information. In *Proceedings of the AAAI Conference on Artificial Intelligence*, volume 39(13), pages 14486–14493, 2025.

## A Additional Qualitative Results of Image Reconstruction

In the main text, we presented representative reconstruction results for Sub-01, Sub-08, and Sub-09. To demonstrate the consistency of STAMBRIDGE across subjects, we provide the qualitative reconstruction results for the remaining seven subjects (Sub-02, Sub-03, Sub-04, Sub-05, Sub-06, Sub-07, and Sub-10) under the rapid serial visual presentation (RSVP) paradigm.

For each subject, the reconstructed images are organized into **Best**, **Median**, and **Worst** cases according to their high-level semantic similarity to the corresponding ground-truth visual stimuli.

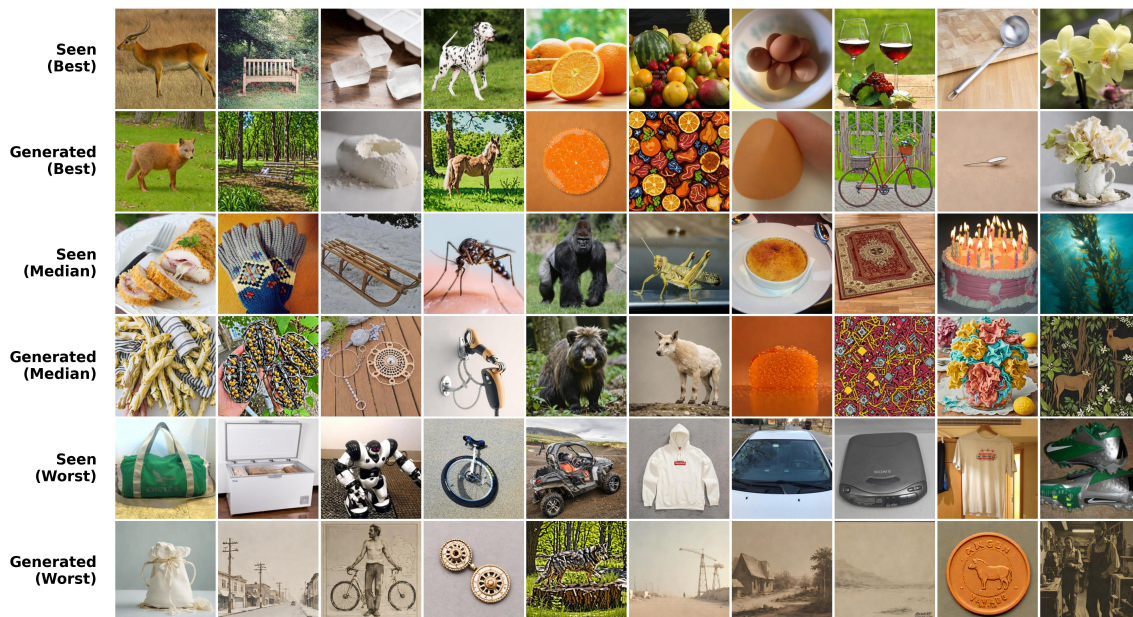


Figure A1: Qualitative results of semantic image reconstruction for Subject 02. The rows correspond to the Best, Median, and Worst reconstruction cases.

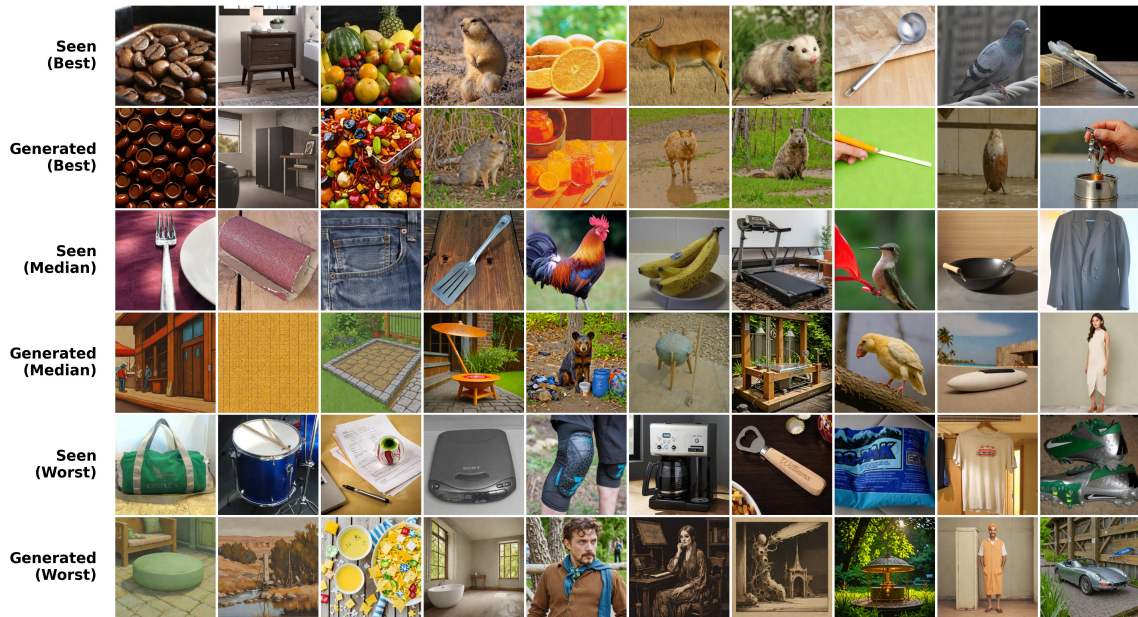


Figure A2: Qualitative results of semantic image reconstruction for Subject 03.

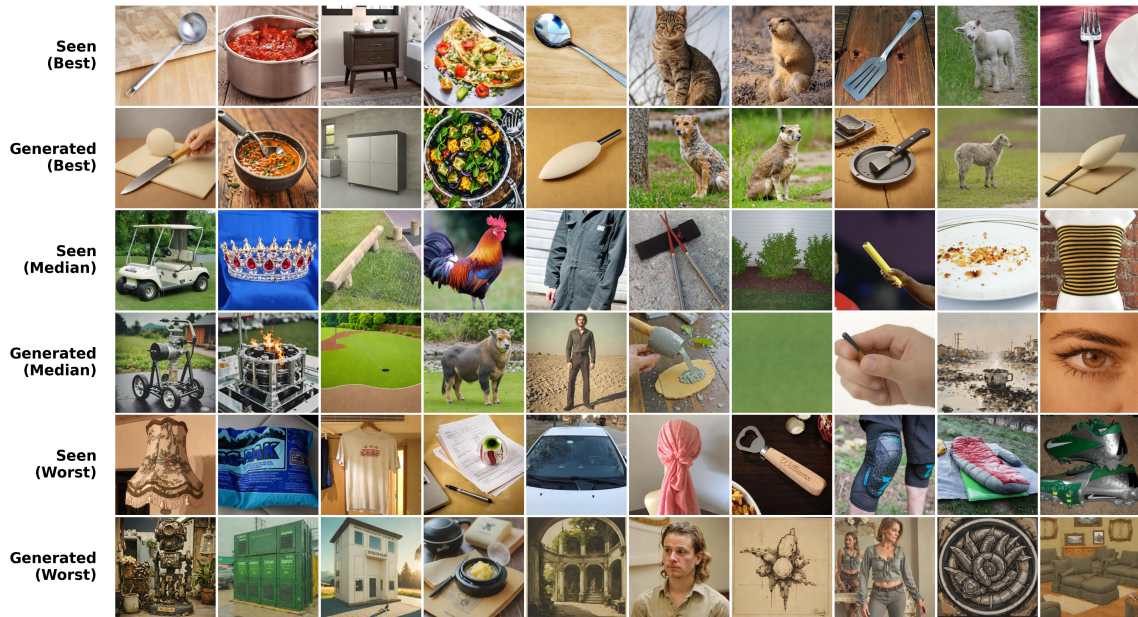


Figure A3: Qualitative results of semantic image reconstruction for Subject 04.

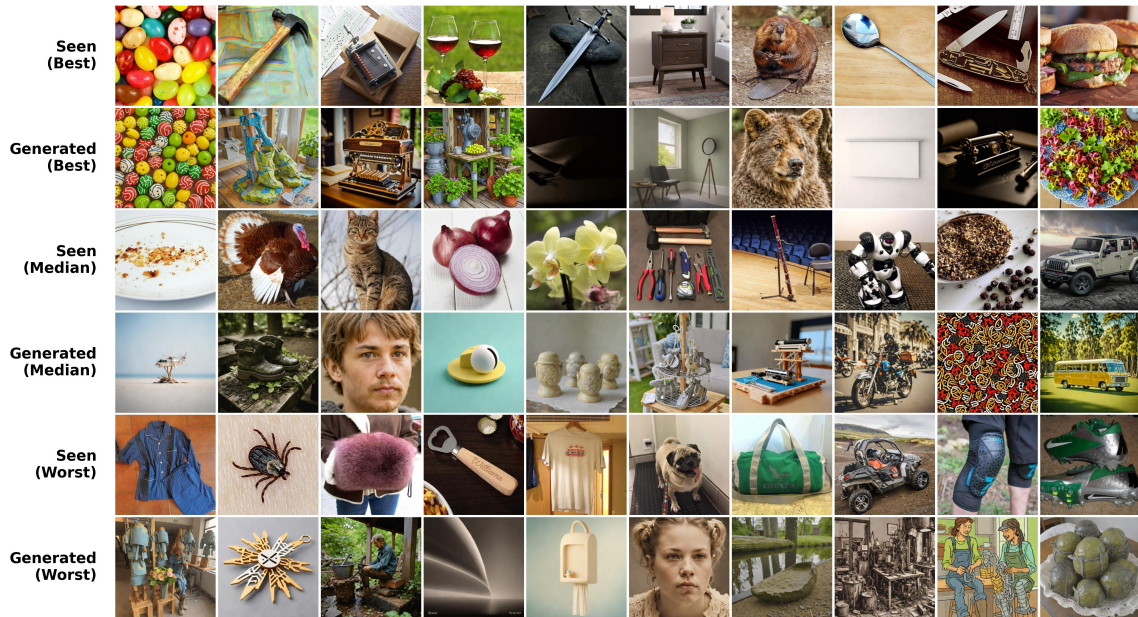


Figure A4: Qualitative results of semantic image reconstruction for Subject 05.

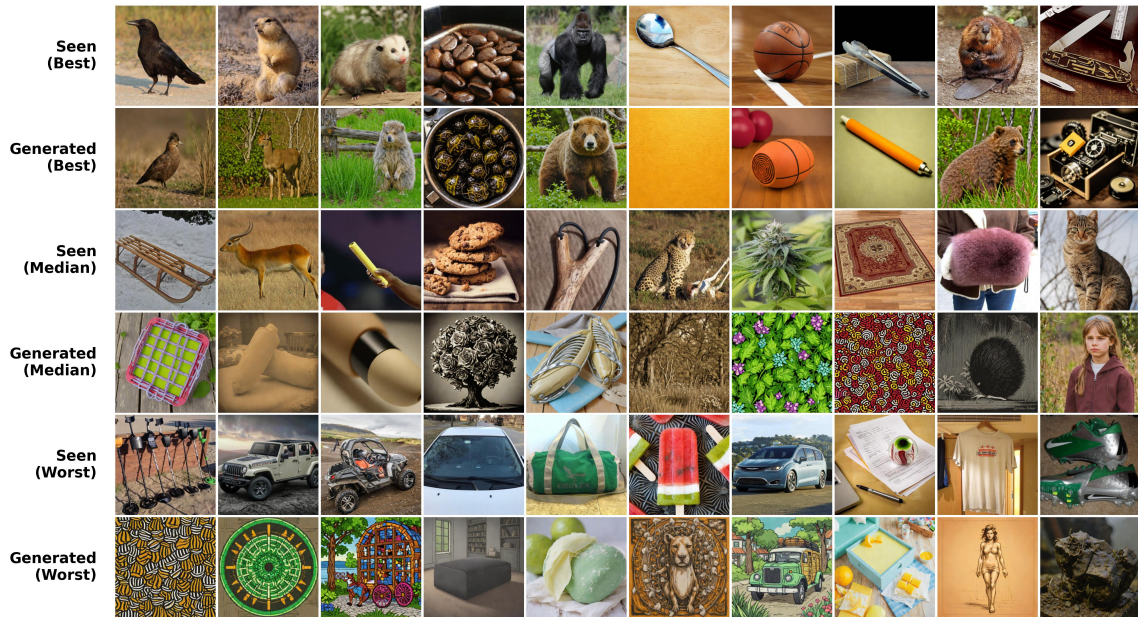


Figure A5: Qualitative results of semantic image reconstruction for Subject 06.

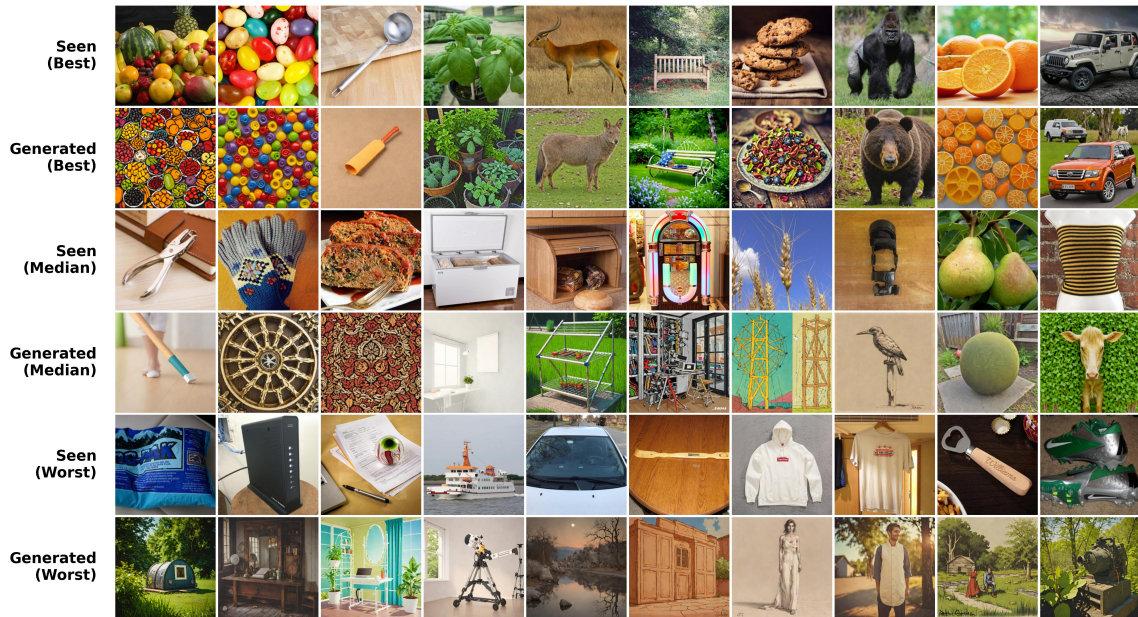


Figure A6: Qualitative results of semantic image reconstruction for Subject 07.

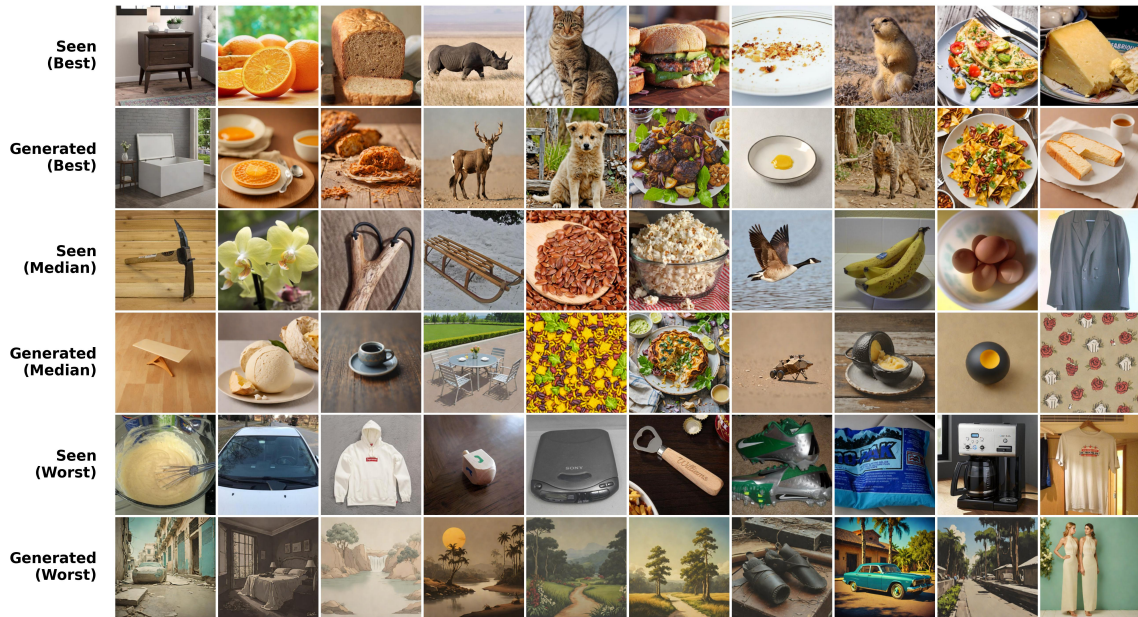


Figure A7: Qualitative results of semantic image reconstruction for Subject 10.